Deuterium dynamics in the icosahedral and amorphous phases of the $Ti_{40}Zr_{40}Ni_{20}$ hydrogen-absorbing alloy studied by ^{2}H NMR

2008 J. Phys.: Condens. Matter 20 475209

(http://iopscience.iop.org/0953-8984/20/47/475209)

J. Phys.: Condens. Matter **20** (2008) 475209 (7pp) doi:10.1088/0953-8984/20/47/475209

Deuterium dynamics in the icosahedral and amorphous phases of the $Ti_{40}Zr_{40}Ni_{20}$ hydrogen-absorbing alloy studied by ^2H NMR

A Gradišek[1], A Kocjan[1], P J McGuiness[1], T Apih[1], Hae Jin Kim[2] and J Dolinšek[1,3]

[1] J Stefan Institute, Jamova 39, SI-1000 Ljubljana, Slovenia
[2] Energy Nano Material Team, Frontier Research Laboratory, Korea Basic Science Institute, 52 Yeoeun, Yuseong, Daejeon 305-333, Republic of Korea
[3] Faculty of Mathematics and Physics, University of Ljubljana, Jadranska 19, SI-1000 Ljubljana, Slovenia

Received 9 September 2008
Published 6 November 2008
Online at stacks.iop.org/JPhysCM/20/475209

Abstract

The $Ti_{40}Zr_{40}Ni_{20}$ hydrogen-absorbing alloy was prepared in the icosahedral and amorphous phases by controlling the rotation speed of the melt–spinning method of sample preparation, and the deuterium dynamics was investigated by ^2H NMR dynamic lineshape and spin–lattice relaxation. The results were analysed by the lineshape and relaxation models that assume deuterium thermally activated hopping within a manifold of different chemical environments. The observed 8% larger activation energy for the deuterium hopping over the interstitial sites and the 10% larger static spectrum width of the amorphous phase, as compared to the icosahedral phase, can be accounted for by the larger deuterium content of the investigated amorphous sample. From the deuterium dynamics point of view, the icosahedral phase is not special with respect to the amorphous modification of the same material.

1. Introduction

It has been demonstrated [1] that Ti- and Zr-based quasicrystals (QCs) exhibit favourable hydrogen-storage properties. The best-studied examples are icosahedral (i) Ti–Zr/Hf–Ni [2–6] and Zr–Cu–Ni–Al [7–14]. The total loading capacity of QCs is competitive with the best known H-storage crystalline alloys (a hydrogen-to-metal ratio H/M $\approx$ 2.0 can be reached, whereas the maximum capacity per weight of 2.5% is less favourable), the absorption and desorption of hydrogen is quick and the alloys are made of low-cost materials. High hydrogen-storage capacity of QCs is considered to originate from the specific atomic cluster structure of these aperiodic compounds [1]. The basic building block of the icosahedral phase is usually a multi-shell atomic cluster of icosahedral symmetry, which aperiodically repeats over the structure. The polytetrahedral local atomic order within these clusters is at the origin of a large number of tetrahedral and octahedral interstitial sites, which are preferentially occupied by hydrogen atoms. For example, the Mackay icosahedral cluster, the building block of the Al–Pd–Mn-type i-QCs and the related crystalline phases in Al–Mn, Ti–Cr–Si–O and Ti–Zr–Fe alloys contains 20 tetrahedral interstitials inside its inner icosahedral shell and 60 tetrahedral interstitials and 20 octahedral interstitials between its inner and outer shells. The Bergman atomic cluster, the building block of the Al–Mg–Zn-type i-QCs and the related icosahedral and crystalline phases in Al–Li–Cu and Ti–Zr–Ni alloys, contains 20 tetrahedral interstitials within its inner shell, 120 between the inner and the outer shells, and no octahedral interstitials.

While the icosahedral cluster structure and the favourable hydrogen chemistry (low binding energy to metal atoms) are at the origin of the excellent H-storage properties of the Ti- and Zr-based i-QCs, it is interesting to compare the hydrogen-related properties of the icosahedral phase to the amorphous phase of the same material in relation to the structural differences of these two phases. The i-QC phase exhibits translationally nonperiodic long-range atomic order

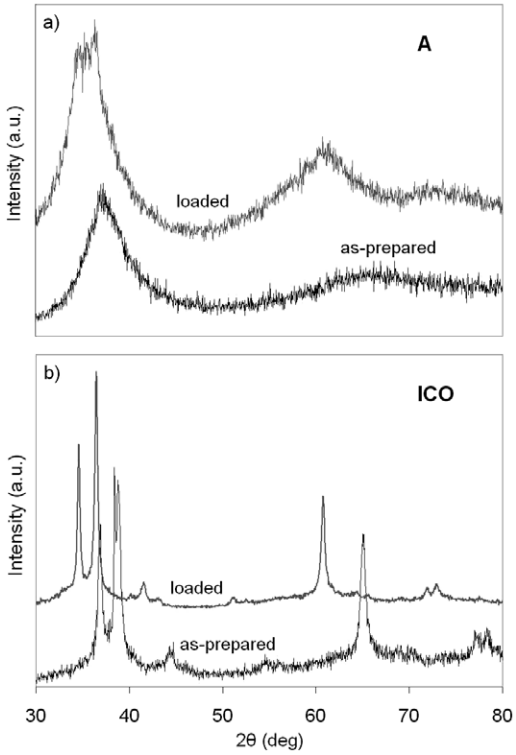

Figure 1. X-ray diffraction spectra of the (a) amorphous (A) and (b) icosahedral (ICO) $Ti_{40}Zr_{40}Ni_{20}$ samples in the as-prepared (unloaded) state and after deuterium loading.

obeying crystallographically forbidden symmetry (fivefold rotation), whereas, in the amorphous phase, long-range order is absent while short-range order on the scale of nearest-neighbour atoms with predominant icosahedral coordination is still believed to be present [15]. A comparative study of the hydrogen behaviour in alloys of the same chemical composition, but of different structural modifications, can be conveniently performed on the $Ti_{40}Zr_{40}Ni_{20}$ alloy, where samples of icosahedral and amorphous phases can be produced from the melt by controlling the rotation speed of the melt–spinning method of sample preparation. In the following we present a study of the temperature-dependent hydrogen dynamics in the above two phases of $Ti_{40}Zr_{40}Ni_{20}$, using the deuterium isotope ^{2}H and nuclear magnetic resonance (NMR) spectroscopy.

2. Sample preparation and characterization

Alloy precursors in the form of two arc-melted buttons (total 9 g) for the melt-spinner (*Edmund Bühler GmbH*) were prepared by the arc-melting of Zr–Ni alloys and Ti powders, in such a ratio that the final material composition of the arc-melted button was $Ti_{40}Zr_{40}Ni_{20}$. These buttons were then placed in the melt-spinner's boron nitride melting crucible, with a 1.5 mm nozzle diameter. After evacuation to 5×10^{-5} mbar using a rotary-turbo vacuum-pump system, the chamber of the melt-spinner was refilled with 99.99% argon gas. The buttons were then heated up to 1400 °C by RF induction, with the temperature measured using a pyrometer

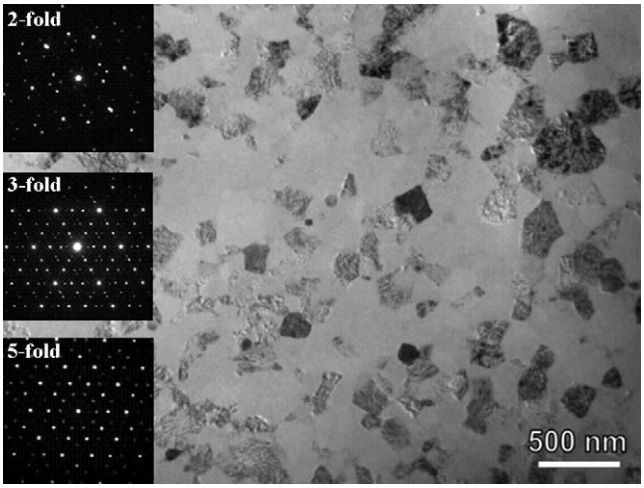

Figure 2. TEM image of the ICO sample, showing quasicrystalline micrograins within the amorphous matrix. The electron diffraction patterns along the two-, three- and fivefold directions of the quasicrystals are also displayed, showing that icosahedral symmetry of the micrograins is well developed.

positioned directly above the melting crucible. After 10–15 s at 1400 °C, the melt was injected through the nozzle using a 200 mbar overpressure of argon onto the melt-spinner's 200 mm diameter rotating copper wheel. The experiment was repeated over a range of different wheel speeds to produce icosahedral and amorphous structures. A fully amorphous phase was obtained for the rotation speed of 32 m s^{-1}, whereas the icosahedral phase formed at 22 m s^{-1}. The structures of the ribbons were confirmed using x-ray diffraction (*D4 Endeavour x-ray diffractometer Bruker AXS*) with Cu Kα radiation in the range from 30° to 80°. The diffraction spectra of the as-prepared samples, together with the corresponding spectra after deuterium loading, are displayed in figure 1. The amorphous and icosahedral structures of the x-ray patterns are clearly discernible. The broadening of the icosahedral peaks at the base reveals that some amorphous phase is still present in the icosahedral sample. In the following we designate the icosahedral sample as ICO and the amorphous sample as A.

For the transmission electron microscopy (TEM), the melt-spun ribbons were cut into discs of 3 mm diameter, which were initially about 50 μm thick. The samples were then subsequently thinned using ion-milling (RES 010, Bal-Tec AG, Balzers, Liechtenstein) with 6 keV Ar^+ ions at an incidence angle of 10° until the central area of the disc was perforated. This was followed by ion polishing using 2 keV Ar^+ ions to produce large, electron-transparent regions with low ion damage to the specimen surface. The TEM analysis (selected-area electron diffraction and bright-field imaging) was made with a JEOL JEM-2100 (Jeol Ltd, Tokyo, Japan) at a 200 kV accelerating voltage. The TEM image of the ICO sample, together with the electron diffraction patterns along the two-, three- and fivefold directions, are displayed in figure 2. We observe that icosahedral grains of up to 500 nm diameter are dispersed within the amorphous matrix with the total icosahedral volume of about 60%. The electron diffraction patterns confirm that the icosahedral symmetry is

well developed. The physical properties of the ICO sample, to be presented in the following, should not be considered as the properties of the icosahedral phase, but of the icosahedral micrograins embedded in an amorphous matrix.

Deuterium loading was performed from the gas phase by exposing the material to the D_2 atmosphere at room temperature and a pressure of 10 bar (ICO sample) or 20 bar (A sample). Under these conditions, the ICO sample absorbed 1.89 wt% of D_2, corresponding to the deuterium-to-metal ratio D/M = 0.64, whereas the A sample absorbed 4.3 wt% of D_2 or D/M = 1.48. The x-ray spectra of the loaded and unloaded samples are displayed in figure 1. The shift of the peaks to lower angles due to the lattice expansion upon deuteration is observed for both samples. For the ICO sample, the peak shift confirms that deuterium has entered the icosahedral micrograins. The x-ray spectrum of the deuterium-loaded A sample shows an additional feature: the high peak at $2\theta \approx 36°$ due to the first-neighbour atomic shell shows some additional structure of sharp lines at its top, demonstrating that a small amount of a crystalline phase (perhaps a stable metal hydride phase) formed within the amorphous matrix upon deuteration.

3. Dynamic NMR lineshape

3.1. Theoretical dynamic NMR lineshape for a distribution of local chemical environments

We consider the effect of the motion of the resonant nuclei on the NMR lineshape in a system with a distribution of local chemical environments, a situation commonly encountered in QCs and amorphous (glassy) structures. The proton NMR lineshape is determined predominantly by the secular part of the nuclear magnetic dipole–dipole interaction, whereas the deuteron lineshape is determined by the magnetic dipole–dipole and the electric quadrupole interactions, with both interactions being traceless. Fast isotropic molecular motions average these interactions to zero, producing a complete motional narrowing of the NMR spectrum at high temperatures, whereas at low temperatures, a static spectrum is observed. The dynamic lineshape transition from the fast- to the slow-motion regime allows extraction of the physical parameters of the motional processes—the correlation time, the activation energy and the distributions of these two parameters in the case that many different motional processes take place simultaneously.

Our choice to perform NMR measurements on the ^{2}H nuclei instead of ^{1}H is based on the following difference between the two isotopes. Protons (spin-1/2 nuclei) possess a strong nuclear magnetic dipole moment but no electric quadrupole moment, so that protons are strongly dipolarly coupled among themselves, but much more weakly to the lattice. In a motional process, the resonance frequency of a proton is predominantly affected by the fluctuating magnetic fields of other protons. This interaction is non-local and hence not specific to a particular lattice site. Deuterons (spin-1 nuclei), on the other hand, possess a factor 6.5 smaller nuclear magnetic dipole moment, making nuclear dipole–dipole interaction between deuterons smaller by a factor $(6.5)^2 \approx 42$. Due to the nonzero electric quadrupole moment, deuterons interact with the electric field gradient (EFG) tensor of the neighbouring charges and the quadrupole interaction dominates over the dipolar one. The EFG is specific to each lattice site. The QC and amorphous structures are characterized by a wide distribution of different local chemical environments, resulting in a distribution of the EFG tensors. Deuteron dynamics involves thermal hopping from one interstitial site to another, so that deuterons probe the distribution of the EFGs (via the inhomogeneous broadening of the NMR spectrum) and the associated distribution of hopping barriers (via the distribution of the hopping rates). Due to the local character of the electric quadrupole interaction, these distributions are more clearly probed by ^{2}H NMR than by the non-locally coupled ^{1}H magnetic moments.

The quantity that determines the temperature-dependent NMR lineshape is the reduced autocorrelation function $g_\omega(t) = \langle\omega(t)\omega(t-\tau)\rangle/\langle\omega^2(t)\rangle$ of the frequency $\omega(t)$ of the fluctuating random fields at the deuteron sites [16]. Here the brackets $\langle\,\rangle$ represent an average over the distribution of frequencies between which the resonance frequency randomly jumps. In the case of a single type of a motional process, the loss of coherence with time is exponential and characterized by a correlation time τ:

$$g_\omega(t) = \exp\{-t/\tau\}. \tag{1}$$

In systems with a complex structure it is often still reasonable to assume that the relaxation is intrinsically exponential, but the large distribution of chemical environments with different characteristics leads to variations in the correlation time τ. When the experiment simultaneously measures a large ensemble of local correlation times, the autocorrelation function may be conveniently described by the empirical stretched exponential Kohlrausch–Williams–Watts (KWW) function [17]:

$$g_\omega(t) = \exp\{-(t/\tau_c)^\alpha\}, \tag{2}$$

where τ_c has the meaning of an average correlation time and α is the 'stretched' exponent ($0 < \alpha < 1$). The stretched exponential function is a Laplace transform of the distribution of correlation times $\rho(\tau)$:

$$\exp\{-(t/\tau_c)^\alpha\} = \int_0^\infty \exp\{-t/\tau\}\,\rho(\tau)\,\mathrm{d}\tau. \tag{3}$$

Knowing τ_c and α, the distribution $\rho(\tau)$ can be reconstructed by performing the inverse Laplace transformation of the stretched exponential function of equation (2).

The NMR lineshape $I(\omega)$ is given by the Fourier transform of the free induction decay function $\tilde{G}(t)$ [16]:

$$I(\omega) = \int \tilde{G}(t)\mathrm{e}^{-\mathrm{i}\omega t}\,\mathrm{d}t. \tag{4}$$

Here

$$\tilde{G}(t) = \mathrm{e}^{\mathrm{i}\omega_0 t}G(t) = \mathrm{e}^{\mathrm{i}\omega_0 t}\left\langle \exp\left[\mathrm{i}\int_0^t \omega(t')\,\mathrm{d}t'\right]\right\rangle, \tag{5}$$

where ω_0 is the nuclear Larmor frequency. $G(t)$ can be expressed as

$$G(t) = \exp\{-\omega_p^2 Z(t)\}, \tag{6}$$

with

$$Z(t) = \int_0^t (t-\tau)\, g_\omega(\tau)\, \mathrm{d}\tau. \tag{7}$$

Here $\omega_p^2 = \langle\omega^2\rangle$ is the second moment of the resonance line for a rigid lattice. Using the stretched exponential autocorrelation function of equation (2), $Z(t)$ can be evaluated analytically as [18]

$$Z(t) = \frac{\tau_c t}{\alpha}\gamma\left[\frac{1}{\alpha}, \left(\frac{t}{\tau_c}\right)^\alpha\right] - \frac{\tau_c^2}{\alpha}\gamma\left[\frac{2}{\alpha}, \left(\frac{t}{\tau_c}\right)^\alpha\right], \tag{8}$$

where γ represents the incomplete gamma function that depends on the value of the stretched exponent α.

In the slow-motion limit ($\omega_p\tau_c \gg 1$), we get $Z(t) \approx t^2/2$ for $\tau_c \to \infty$ and

$$G(t) \approx \exp\left\{-\tfrac{1}{2}\omega_p^2 t^2\right\}, \tag{9}$$

yielding a Gaussian lineshape with the α-independent standard deviation ω_p. In the fast-motion limit ($\omega_p\tau_c \ll 1$), we get, on the other hand, $Z(t) \approx \tau_c t\,\Gamma(1/\alpha + 1)$ for $\tau_c \to 0$, where Γ is the complete gamma function and

$$G(t) = \exp\left\{-\omega_p^2\tau_c\,\Gamma\left(\frac{1}{\alpha}+1\right)t\right\}, \tag{10}$$

yielding a Lorentzian lineshape, the width of which depends on the value of the stretched exponent α. Since at high temperatures $\tau_c \to 0$, the asymptotic Lorentzian lineshape in the fast-motion limit becomes infinitely narrow. Equation (6) can be adapted to yield a nonzero residual linewidth in this limit by splitting the second moment into two parts: $\omega_p^2 = \omega_p'^2 + \omega_p''^2$. Here only the $\omega_p'^2$ term is destroyed by the motion, whereas the $\omega_p''^2$ term represents the residual linewidth at high temperatures, originating from the interactions that are not averaged to zero by the motion. This is the case for the anisotropic molecular motions, where not all of the EFG tensor elements are averaged to zero and the motional narrowing of the spectrum is incomplete. The nonzero residual linewidth at high temperatures is often determined by the external magnetic field inhomogeneity. Using the above modification of the second moment, equation (6) can be rewritten as

$$G(t) = \exp\left\{-\tfrac{1}{2}\omega_p''^2 t^2\right\}\exp\{-\omega_p'^2 Z(t)\}, \tag{11}$$

yielding a Gaussian asymptotic lineshape in the fast-motion limit with the standard deviation ω_p''.

3.2. Comparison with the experiment

The ^{2}H NMR lineshape measurements were performed in a cooling run from 400 to 77 K at the deuterium Larmor frequency $\nu_0(^2\mathrm{H}) = 30.701$ MHz. The temperature-dependent NMR spectra of the ICO and A samples are displayed in figure 3, showing a dynamic transition from a motionally narrowed spectrum above 300 K to a static spectrum below about 200 K. While the shape of the static spectrum is nearly Gaussian (figure 3(c)), the asymptotic high-temperature lineshape is Lorentzian (figure 3(d)). Our samples are polygrain ribbons, so that the static spectrum corresponds to that of a crystalline powder. The fact that the static ^{2}H spectra of the ICO and A samples exhibit a Gaussian shape, instead of showing a quadrupole asymmetry parameter η-dependent singularities typical of a ^{2}H crystalline powder spectrum, suggests that the EFG principal values and η are distributed due to a distribution of the local chemical environments.

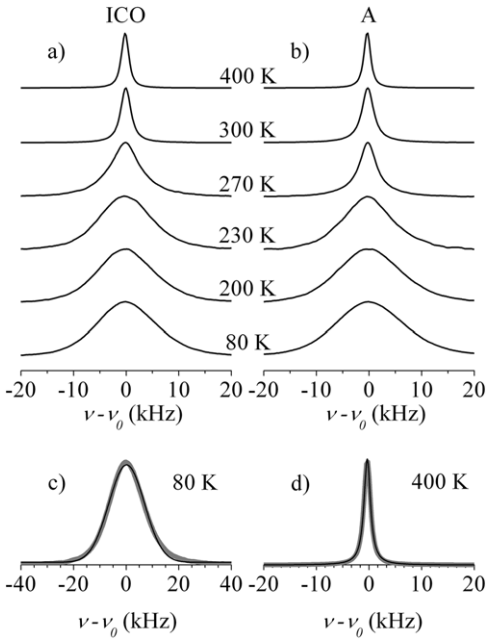

Figure 3. The temperature-dependent deuterium NMR spectra of (a) the ICO sample and (b) the A sample. For the A sample, the Gaussian fit of the static spectrum at $T = 80$ K is shown in (c), whereas a Lorentzian fit of the motionally narrowed spectrum at $T = 400$ K is shown in (d) (the experimental data are shown by thick grey curves whereas the thin black curves are theoretical).

The temperature-dependent full width at half-maximum (FWHM) of the ^{2}H spectra is displayed in figure 4. For both samples, the transition from the fast- to the slow-motion regime occurs in the temperature range roughly between 300 and 200 K. The high-temperature asymptotic FWHMs for both samples amount to 1.1 kHz, which is considerably higher than our magnet inhomogeneity, so that not all nuclear spin interactions are averaged to zero by fast molecular motions. For the ICO sample, the FWHM of the static spectrum amounts to 13 kHz, whereas it amounts to 15 kHz for the A sample. Assuming that the motional processes can be attributed to the deuterium hopping between neighbouring interstitial sites, this demonstrates that the deuterium hopping frequencies slow down upon cooling and cross the 1–10 kHz range between 300 and 200 K. The analysis of the temperature-dependent FWHMs was performed by fitting the experimental lineshapes to equations (4) and (11) and then extracting the full width at 50% height. We assumed an Arrhenius thermally activated form of the autocorrelation time, $\tau_c = \tau_0\exp(E_a/k_BT)$, with the activation energy E_a. For the ICO sample, the following

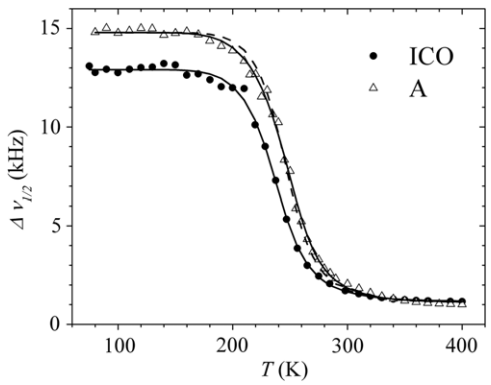

Figure 4. The temperature-dependent full width at half-maximum (FWHM) $\Delta\nu_{1/2}$ of the ^{2}H NMR spectra of the ICO and A samples. Solid lines are fits with equations (4) and (11), using a stretched exponential autocorrelation function of equation (2) with $\alpha = 0.80$. The fit with the mono-dispersive autocorrelation function of equation (1), corresponding to $\alpha = 1$, is shown by a dashed line for the A sample. The fitting parameter values are given in the text.

parameter values were determined from the fit (solid curve in figure 4): $\tau_0 = (2 \pm 1) \times 10^{-10}$ s, $E_a = 230 \pm 10$ meV, $\omega'_p = 2\pi \times 5.4$ kHz, $\omega''_p = 2\pi \times 0.5$ kHz and $\alpha = 0.78 \pm 0.15$. In the fitting procedure, the parameters τ_0, E_a and α slightly compensate for each other (the compensation between τ_0 and α being larger), so that we give ranges of their values within which equally good fits could be obtained. For the A sample, the fitting parameters are $\tau_0 = (2 \pm 1) \times 10^{-10}$ s, $E_a = 250 \pm 10$ meV, $\omega'_p = 2\pi \times 6.2$ kHz, $\omega''_p = 2\pi \times 0.5$ kHz and $\alpha = 0.80 \pm 0.15$. Comparing the above figures, we observe that the parameters τ_0 and α of the ICO and A samples are practically the same. Sample A exhibits about 10% larger static spectrum width (stronger inhomogeneous broadening), suggesting that the manifold of different local chemical environments in the amorphous phase is somewhat larger than in the icosahedral phase, but the difference is relatively small. This difference can be a consequence of the fact that the deuterium content of the A sample (D/M = 1.48) is larger than that of the ICO sample (D/M = 0.64). Deuterium loading results in an expansion of the lattice and the creation of defects, so that more different local chemical environments (and hence different EFGs at the ^{2}H sites) are expected for the larger deuterium content. The small difference in the activation energies of the ICO and A samples can also be qualitatively understood in terms of their different D/Ms. For hydrogen hopping in the Zr–Cu–Ni–Al amorphous and quasicrystalline state it was shown [13, 14] that the activation energy depends on the hydrogen content. More hydrogen in a metal hydride results in larger expansion of the lattice, and the increased distances between the atoms result in increased hopping barriers. For the amorphous $Zr_{69.5}Cu_{12}Ni_{11}Al_{7.5}$, the activation energy was reported to increase by 15% from H/M = 0.05 to 1.5. For our $Ti_{40}Zr_{40}Ni_{20}$, the E_a difference between the ICO and A samples is a factor $E_a^A/E_a^{ICO} = 1.08$. Since D/M(A) = 1.48 and D/M(ICO) = 0.64, the 8% increase of the activation energy of the A sample with respect to the ICO sample is within expectations for the E_a increase due to the increased D/M.

4. NMR spin–lattice relaxation

4.1. ^{2}H NMR spin–lattice relaxation for a distribution of chemical environments

While the dynamic NMR lineshape is sensitive to molecular motions in the 1–100 kHz frequency window, the NMR spin–lattice relaxation rate T_1^{-1} probes motions with MHz frequencies in the vicinity of the nuclear Larmor frequency, in our case around $\nu_0(^2\mathrm{H}) = 30.701$ MHz. For the thermally activated deuterium hopping, T_1^{-1} is expected to sense the same motion as the dynamic NMR lineshape, but at higher temperatures, when the hopping frequencies speed up from the kHz to the MHz range.

The ^{2}H spin–lattice relaxation rate in an electrically conducting metal hydride is, to a good approximation, given by

$$T_1^{-1} = T_{1Q}^{-1} + T_{1e}^{-1}. \tag{12}$$

Here T_{1Q}^{-1} is the electric quadrupolar rate due to fluctuating EFG tensor elements and T_{1e}^{-1} arises from fluctuations of the hyperfine interaction between the nuclear spins and the spins of conduction electrons. The contributions from the fluctuating dipolar interaction and the possible presence of paramagnetic impurities have been neglected in comparison to the other two contributions. T_{1e}^{-1} obeys the Korringa form $T_{1e}T = \text{const.}$ and can be written as

$$T_{1e}^{-1} = KT. \tag{13}$$

The quadrupolar rate is written as [19]

$$T_{1Q}^{-1} = \frac{3}{80}\left(\frac{e^2Qq}{\hbar}\right)^2\left(1 + \frac{\eta^2}{3}\right)[J(\omega_0) + 4J(2\omega_0)], \tag{14}$$

where η is the quadrupole asymmetry parameter, $eq = V_{ZZ}$ is the largest eigenvalue of the EFG tensor and Q is the nuclear electric quadrupole moment. $J(\omega_0)$ and $J(2\omega_0)$ are the spectral densities of the reduced autocorrelation function $g_\omega(t)$ at the Larmor frequency ω_0 given by

$$J(\omega) = 2\int_0^\infty g_\omega(t)\cos\omega t \, \mathrm{d}t. \tag{15}$$

For a simple motional process characterized by a single correlation time τ, $g_\omega(t)$ is given by equation (1) and $J(\omega)$ becomes

$$J(\omega) = \frac{2\tau}{1 + \omega^2\tau^2}. \tag{16}$$

For the stretched exponential autocorrelation function of equation (2), the integration in equation (15) can be calculated analytically only in the fast-motion ($\omega\tau_c \ll 1$) and slow-motion ($\omega\tau_c \gg 1$) limits [20]:

$$J(\omega) = 2\Gamma\left(\frac{1}{\alpha} + 1\right)\tau_c, \qquad \omega\tau_c \ll 1 \tag{17a}$$

$$J(\omega) = \frac{2\Gamma(\alpha + 1)\sin(\pi\alpha/2)}{\omega^{\alpha+1}\tau_c^\alpha}, \qquad \omega\tau_c \gg 1 \tag{17b}$$

whereas between these two limits the spectral density has to be calculated by a numerical integration of equation (15). Within the slow-motion regime, T_{1Q}^{-1} of equation (14) becomes

$$T_{1Q}^{-1} = \frac{C}{\omega_0^{\alpha+1}\tau_c^{\alpha}}, \tag{18}$$

where $C = (3/40)(e^2Qq/\hbar)^2(1+\eta^2/3)\Gamma(\alpha+1)\sin(\pi\alpha/2)(1+4/2^{\alpha+1})$. Assuming an Arrhenius form of the correlation time τ_c, T_{1Q} exhibits an α-dependent low-temperature slope $\alpha E_a/k_B$ when presented in a $\log T_{1Q}$ versus $1/T$ plot. In the fast-motion limit, on the other hand, the spectral density of equation (17*a*) yields an α-independent negative slope $-E_a/k_B$. Since $0 < \alpha < 1$, the slope on the low-temperature side of the minimum in T_{1Q} (occurring roughly at $\omega_0\tau_c \approx 0.6$) is smaller by a factor α from that on the high-temperature side.

4.2. Comparison to the experiment

The ^{2}H T_1 experiments were conducted in the temperature range between 430 and 77 K, using an inversion-recovery technique. In figure 5(a), the data are displayed in the $(T_1T)^{-1}$ versus T plot, which enables the extraction of the conduction-electron rate from the low-temperature $(T_1T)^{-1} =$ const. plateau. At low temperatures, deuterium motion and the associated EFG fluctuations freeze, so that T_{1Q}^{-1} becomes negligible and $T_1^{-1} \approx T_{1e}^{-1}$, from where we get the Korringa constant $K = (T_{1e}T)^{-1} = 5.7 \times 10^{-4}$ s^{-1} K^{-1} for the ICO sample and $K = 5.0 \times 10^{-4}$ s^{-1} K^{-1} for the A sample. Knowing T_{1e}^{-1}, the quadrupolar rate T_{1Q}^{-1} can be extracted from the total relaxation rate using equations (12) and (13). The quadrupolar contribution is displayed in figure 5(b) in a $\log T_{1Q}$ versus $1000/T$ plot, where two features are evident: (1) in the whole investigated temperature range, the T_{1Q} slope is positive, revealing that the EFG fluctuation frequencies are in the slow-motion regime with respect to the nuclear Larmor frequency and (2) there are two distinctly different temperature regions regarding the T_{1Q} slope, where the slope in the high-temperature region between 430 and 200 K is considerably larger than that in the low-temperature regime between 200 and 77 K. This change of slope indicates the presence of two different kinds of dynamic processes in the samples, one being dominant above 200 K and the other one below. Since both processes yield straight lines in the $\log T_{1Q}$ versus $1000/T$ plot, they are both classical thermally activated processes, but with different activation energies, to be analysed next.

We assume that one type of dynamic process is the deuteron hopping between the manifold of interstitial sites, where T_{1Q}^{-1} is described by equation (18). For the other process, we assume that it is a simple thermally activated process with an activation energy E_{a2}. In the slow-motion limit, T_{1Q}^{-1} can be written as

$$\frac{1}{T_{1Q}} = A_1 \exp\left(-\frac{\alpha E_a}{k_B T}\right) + A_2 \exp\left(-\frac{E_{a2}}{k_B T}\right). \tag{19}$$

The fits with equation (19) are shown as solid curves in figure 5(b). For the ICO sample we obtain parameter values $A_1 = 1.74 \times 10^3$ s^{-1}, $A_2 = 8.25$ s^{-1}, $E_{a2} = 64$ meV

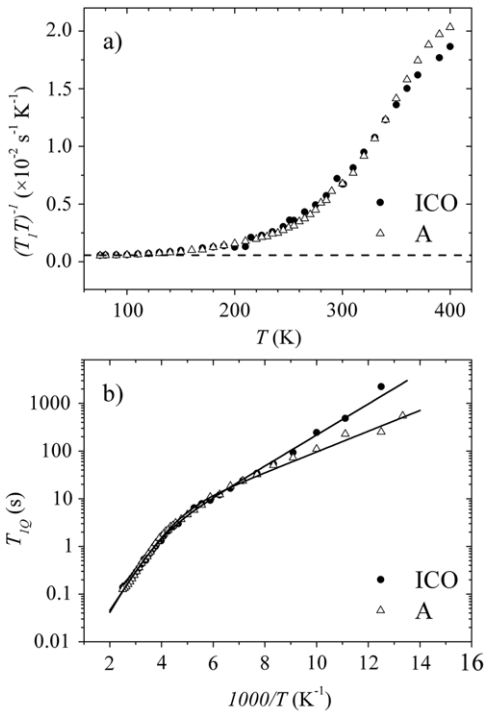

Figure 5. (a) Temperature dependence of the total ^{2}H NMR spin–lattice relaxation rate T_1^{-1} of the ICO and A samples in a $(T_1T)^{-1}$ versus T plot. The low-temperature $(T_1T)^{-1} =$ const. plateau, used for the extraction of the Korringa constant, is shown by a dashed line for the A sample. (b) Temperature dependence of the quadrupolar relaxation rate T_{1Q}^{-1}, presented in a $\log T_{1Q}$ versus $1000/T$ plot. Solid curves are fits with equation (19) and the fitting parameter values are given in the text. Two temperature ranges with markedly different activation energies are discernible.

and, using the range of stretched exponential values $\alpha = 0.78 \pm 0.15$ determined from the dynamic lineshape transition, $E_a = 230 \pm 40$ meV. For the A sample we obtain $A_1 = 1.03 \times 10^3$ s^{-1}, $A_2 = 1.57$ s^{-1}, $E_{a2} = 43$ meV and, using the range $\alpha = 0.80 \pm 0.15$ from the dynamic lineshape transition, $E_a = 240 \pm 40$ meV. Dynamic processes associated with the activation energy E_a are obviously the same as those driving the dynamic lineshape transition (the T_{1Q}-determined E_a values match well those determined from the dynamic lineshape transition).

Regarding the second thermally activated dynamic process described by the activation energy E_{a2}, the values 64 meV for the ICO and 43 meV for the A sample are much smaller than those for the deuterium hopping between interstitial sites. These dynamic processes should be associated with degrees of freedom other than interstitial hopping. The microscopic nature of these processes is not clear, but additional sharp peaks around $2\theta \approx 36°$ in the x-ray spectrum of the deuterium-loaded A sample in figure 1 demonstrate that some deuterons are bound in stable hydride phases, where the deuterons can jump in hydrogen-bond-type double-well potentials over smaller barriers. Typical activation energies for deuteron jumps in hydrogen bonds are about 70 meV (depending on the length of the H-bond), which is of the same order of magnitude as the values observed in our Ti–Zr–Ni samples.

5. Summary and conclusions

The hydrogen-absorbing $Ti_{40}Zr_{40}Ni_{20}$ alloy was prepared in the icosahedral and amorphous phases by controlling the rotation speed of the melt–spinning method of sample preparation and the deuterium dynamics was investigated by the ^{2}H NMR dynamic lineshape and the spin–lattice relaxation. The results were analysed by the lineshape and relaxation models that assume deuterium thermally activated hopping within a manifold of the different chemical environments. The main aim of the study was to see whether the structural state of the $Ti_{40}Zr_{40}Ni_{20}$ phase—icosahedral quasicrystalline or amorphous—plays a significant role in the deuterium (or hydrogen) dynamics in this alloy. No significant differences between the two structural modifications of the same alloy were found. The observed 8% larger activation energy for the deuterium hopping among the interstitial sites and the 10% larger static spectrum width of the amorphous phase, as compared to the icosahedral phase, can be accounted for by the larger deuterium content of the investigated amorphous sample. From the deuterium dynamics point of view, the icosahedral phase is not special compared to the amorphous modification of the same material. This is in agreement with the recently reported investigations of the amorphous and icosahedral $Zr_{69.5}Cu_{12}Ni_{11}Al_{7.5}$ alloy [13, 14], where the same conclusion was reached. Our results suggest that short-range atomic order on the scale of nearest-neighbour atoms exists in the amorphous phase as well and is not much different from that of the quasicrystalline phase. The fact that our isocahedral sample consists of icosahedral quasicrystalline micrograins within a sea of amorphous material with a total icosahedral volume of about 60% may add to the similarity of the investigated amorphous and icosahedral samples. Since the deuterium-loading-induced shift of the icosahedral lines to lower angles in the x-ray spectrum confirms that deuterium has entered quasicrystalline micrograins, a large part of the NMR signal is coming from the icosahedral phase, so that the comparison of the amorphous and icosahedral samples is meaningful. Hydrogen loading into the icosahedral phase results in an increased structural disorder [11], adding to the similarity of the amorphous and icosahedral phases after the deuterium loading.

References

[1] See, for a review Gibbons P C and Kelton K F 1999 *Physical Properties of Quasicrystals* (*Springer Series in Solid-State Sciences* vol 126) ed Z M Stadnik (Berlin: Springer) p 403

[2] Viano A M, Stroud R M, Gibbons P C, McDowell A F, Conradi M S and Kelton K F 1995 *Phys. Rev.* B **51** 12026

[3] Shastri A, Majzoub E H, Borsa F, Gibbons P C and Kelton K F 1998 *Phys. Rev.* B **57** 5148

[4] Faust K R, Pfitsch D W, Stojanovich N A, McDowell A F, Adolphi N L, Majzoub E H, Kim J Y, Gibbons P C and Kelton K F 2000 *Phys. Rev.* B **62** 11444

[5] Foster K, Leisure R G, Shaklee J B, Kim J Y and Kelton K F 2000 *Phys. Rev.* B **61** 241

[6] McDowell A F, Adolphi N L and Sholl C A 2001 *J. Phys.: Condens. Matter* **13** 9799

[7] Köster U, Meinhardt J, Roos S and Liebertz H 1996 *Appl. Phys. Lett.* **69** 179

[8] Wehner B I, Meinhardt J, Köster U, Alves H, Eliaz N and Eliezer D 1997 *Mater. Sci. Eng.* A **226–228** 1008

[9] Zander D, Leptien H, Köster U, Eliaz N and Eliezer D 1999 *J. Non-Cryst. Solids* **250–252** 893

[10] Zander D, Köster U, Eliaz N, Eliezer D and Plachke D 1999 *Mater. Res. Soc. Symp. Proc.* vol 553, ed J M Dubois, P A Thiel, A P Tsai and K Urban (Warrendale: Materials Research Society) p 49

[11] Zander D, Köster U and Khare V 2001 *Mat. Res. Soc. Symp. Proc.* vol 643, ed E Belin-Ferré, P A Thiel, A P Tsai and K Urban (Warrendale: Materials Research Society) p K2.2.1

[12] Apih T, Khare V, Klanjšek M, Jeglič P and Dolinšek J 2003 *Phys. Rev.* B **68** 212202

[13] Apih T, Bobnar M, Dolinšek J, Jastrow L, Zander D and Köster U 2005 *Solid State Commun.* **134** 337

[14] Dolinšek J, Apih T, Klanjšek M, Kim H J and Köster U 2007 *Catal. Today* **120** 351

[15] Luo W K, Sheng H W, Alamgir F M, Bai J M, He J H and Ma E 2004 *Phys. Rev. Lett.* **92** 145502

[16] Abragam A 1961 *The Principles of Nuclear Magnetism* (Oxford: Oxford University Press) p 439

[17] Williams G and Watts D C 1970 *Trans. Faraday Soc.* **66** 80

[18] Dolinšek J, Koren M and Kind R 1998 *Phys. Rev.* B **57** 2812

[19] Abragam A 1961 *The Principles of Nuclear Magnetism* (Oxford: Oxford University Press) p 314

[20] Korner N H 1993 *Diss. ETH No. 9952* (Switzerland: ETH Zurich) p 50